



**HAL**  
open science

## Efficient concentration of high-energy x-rays for diffraction-limited imaging resolution

Julio Cesar da Silva, Alexandra Pacureanu, Yang Yang, Sylvain Bohic, Christian Morawe, Raymond Barrett, Peter Cloetens

► **To cite this version:**

Julio Cesar da Silva, Alexandra Pacureanu, Yang Yang, Sylvain Bohic, Christian Morawe, et al.. Efficient concentration of high-energy x-rays for diffraction-limited imaging resolution. *Optica*, 2017, 4 (5), pp.492-495. 10.1364/OPTICA.4.000492 . hal-01691891

**HAL Id: hal-01691891**

**<https://hal.science/hal-01691891>**

Submitted on 24 Jan 2018

**HAL** is a multi-disciplinary open access archive for the deposit and dissemination of scientific research documents, whether they are published or not. The documents may come from teaching and research institutions in France or abroad, or from public or private research centers.

L'archive ouverte pluridisciplinaire **HAL**, est destinée au dépôt et à la diffusion de documents scientifiques de niveau recherche, publiés ou non, émanant des établissements d'enseignement et de recherche français ou étrangers, des laboratoires publics ou privés.

# Efficient concentration of high-energy x-rays for diffraction-limited imaging resolution

JULIO CESAR DA SILVA,<sup>1,\*</sup> ALEXANDRA PACUREANU,<sup>1</sup> YANG YANG,<sup>1</sup> SYLVAIN BOHIC,<sup>1,2</sup> CHRISTIAN MORAWE,<sup>1</sup> RAYMOND BARRETT,<sup>1</sup> AND PETER CLOETENS<sup>1</sup>

<sup>1</sup>European Synchrotron Radiation Facility, Grenoble 38000, France

<sup>2</sup>INSERM U836, (Team 6: Synchrotron Radiation and Medical Research), Grenoble Institute of Neuroscience, Grenoble 38000, France

\*Corresponding author: [jasilva@esrf.fr](mailto:jasilva@esrf.fr)

Received 3 January 2017; revised 20 March 2017; accepted 21 March 2017 (Doc. ID 283830); published 24 April 2017

**Newly available x-ray nanobeams in synchrotron radiation facilities open new research avenues in the nanosciences. However, a significant challenge is to efficiently concentrate, particularly for high-energy x-rays, a large photon flux into a very small focal spot. Here, we demonstrate for the first time, to the best of our knowledge, a sub-13-nm (FWHM) diffraction-limited x-ray focus size with 6 billion photons per second formed using elliptically figured mirrors operating at 33.6 keV. This is the smallest and brightest focus spot in this high-energy range. We report the results of an x-ray ptychography experiment to characterize the wavefront at the focus position. This offers new opportunities in multidisciplinary fields for x-ray microscopy techniques in which the focal spot size limits the resolution.** © 2017 Optical Society of America

**OCIS codes:** (000.3110) Instruments, apparatus, and components common to the sciences; (070.7345) Wave propagation; (110.7440) X-ray imaging; (180.7460) X-ray microscopy; (340.7470) X-ray mirrors.

<https://doi.org/10.1364/OPTICA.4.000492>

X-ray nanobeams are a powerful tool for the characterization of the local structure and composition of heterogeneous specimens by scanning x-ray fluorescence (XRF) and diffraction microscopy techniques [1–3]. In many cases, the resolution of the image is limited by the size of the focused spot [3–6], which is limited by the quality of the focusing optics. The power of mapping elemental composition down to trace elements in materials using XRF at the microscale has already been widely recognized [5,7–9]. However, many technologically important materials or biological samples are structurally inhomogeneous across multiple length scales down to nanometer level. The availability of x-ray nanoprobes plays a key role in the exploration of such systems at the nanoscale and enables the transition from average ensemble measurements to precise local characterization of the environment and of deviations from average behavior [2].

The detection limit of elements by XRF and the detection power of diffraction peaks of tiny structures are synergistically improved by using a smaller x-ray beam with an increased photon

flux. Furthermore, the use of high-energy x-rays (>20 keV), apart from extending the range of detectable elements, allows improved penetration of the probe into either thick or highly absorbing samples. However, the available focusing optics in the hard x-ray domain typically presents a decreasing efficiency with increasing energy. Consequently, it is particularly challenging to produce nanometer-scale x-ray probes with high flux at energies above 20 keV.

Highly brilliant x-ray sources such as current third-generation synchrotrons or future diffraction-limited storage rings and x-ray free-electron lasers are exquisite candidates to produce intense nanobeams pending the development of adapted focusing optics. The most commonly used focusing systems are based on Kirkpatrick–Baez (KB) mirrors [10], zone plates [11] or compound refractive optics [12]. Despite the ease of use of zone plates and compound refractive optics compared with KB mirrors, their efficiency is generally low at photon energies above 20 keV. Multilayer Laue lenses [13,14] are a promising planar variation on the zone-plate approach, which, due to volume diffraction, can offer high efficiency at high energies. However, their application is complicated due to short focal distances. Furthermore, their small aperture and the high monochromaticity required limit the focused flux. Curved mirrors used in the KB geometry are a well-established focusing device and, through constant technological advances, currently present the most efficient method for the formation of nanometer-scale hard x-ray beams. An x-ray beam focused in one direction to 7 nm at 20 keV using KB mirrors has been demonstrated by combining adaptive optics, multilayer mirrors and ultrasmooth, near-atomic polishing methods [15]. However, the challenge of obtaining a two-dimensional (2D) sub-30 nm focus size at energies above 20 keV has not been demonstrated previously.

The biggest challenges to obtain nanobeams with KB mirrors are the sub-nanometer manufacturing requirements on the substrate shapes, the angular alignment and the stability of the mirrors (typically down to 0.1  $\mu$ rad and 10  $\mu$ rad for, respectively, incidence and orthogonality). Any deviations will lead to (spherical) aberrations and astigmatism in the wavefront, and to a blurred focus. In addition, the focused beam size in the hard x-ray range is often determined by scanning the sharp edge of very

narrow lithographic structures or a highly absorbing knife edge perpendicular to the optical axis through the beam focus while measuring either the x-ray absorption or fluorescence intensity of a constituent element of the structure. It is technologically difficult to fabricate sufficiently sharp edges at the nanometer scale and, consequently, such measurements provide only an upper bound limit of the beam size. Therefore, alternative methods must be used in order to determine with better precision the focal spot size [16].

Here, we report a diffraction-limited focal spot of less than 13 nm size (FWHM) formed using 33.6 keV x-rays and graded multilayer coated KB mirrors [17] installed permanently in the new European Synchrotron Radiation Facility (ESRF) end station ID16A dedicated to nanoimaging experiments. This is the smallest x-ray focus ever made using hard x-rays above 20 keV. The elliptical cylinder substrates were purchased from JTEC Corporation, Japan [18]. They consist of Silicon (Si) substrates with dimensions of 36 mm × 20 mm × 20 mm and 70 mm × 20 mm × 20 mm for the horizontal and vertical mirrors, respectively. The short-radius optics were prepared using deterministic figuring/polishing techniques based on technologies developed at Osaka University (elastic emission machining and microstitching interferometry). The mirrors were coated at the ESRF with 120 layers  $W/B_4C$  and integrated into an in-house designed optomechanical assembly. Additional details of the design of the graded multilayer for the specific KB optics can be found in Morawe *et al.* [17]. The focal spot has been characterized not only by sharp-edge scans, but also by high-energy x-ray ptychography, which corresponds to the ptychography experiment with the highest x-ray energy ever performed. An XRF imaging experiment was also performed with a lithographic sample in the focus and the image obtained could be deconvolved using the beam retrieved by ptychography, after Fresnel propagation to the focus position. All this demonstrates the usability of the hard x-ray nanofocusing device and paves the way to sub-20-nm-resolution microscopy on thick samples, reaching a resolution level that goes beyond super-resolution microscopy [19,20], with applications to opaque and thick samples without the need of any optical fluorescence markers. The methods and optics are further described in Supplement 1.

Figure 1(a) shows a sketch of the focusing optics. We carried out scans across a sharp edge of a 10-nm-thick square lithographic structure of 20 μm × 20 μm, made from Nickel (Ni) deposited on a 500-nm-thick silicon nitride membrane; the online visible light micrograph of the structure is shown in Fig. 1(b). Using aperture defining slits of 215 μm × 250 μm ( $H \times V$ ) upstream from the KB, we measured a focal spot size (FWHM) of 24.9 nm in the horizontal and 19.5 nm in the vertical direction, still above the diffraction limit of 6.5 nm × 13 nm ( $H \times V$ ). Figures 1(c) and 1(d) show the resulting curves with the corresponding sigmoidal-like function fits. A true determination of beam size requires a structure with infinitely sharp edges and an assumption that the beam intensity profile is close to Gaussian. For beams deviating from such a shape, this method leads to overestimates of the beam size [21].

The beam intensity profile is better characterized using ptychography [22–26]. Since the complex-valued wavefront at the sample position can be retrieved [22,24], the beam in the focus can be obtained by Fresnel propagation [27] of the beam from the sample to the focus position. The ptychographic scans were

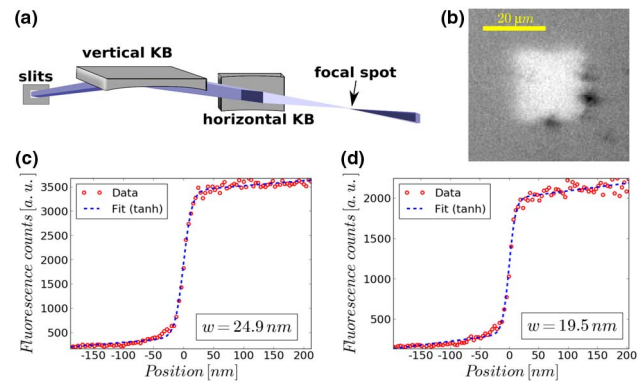


**Fig. 1.** KB mirror focusing optics and edge scans across a 10-nm-thick lithographic structure of 20 μm × 20 μm dimension, made from Nickel deposited on a thin silicon nitride membrane. (a) Sketch of the KB mirror optics. (b) Light micrograph of the lithographic structure. (c) Horizontal scan across a vertical edge of a Ni square. The spot size resulting from the fitting is 24.9 nm. (d) Vertical scan across a horizontal edge of a Ni square. The spot size resulting from the fitting is 19.5 nm.

performed using a gold structure with small lithographically fabricated features as shown in the reconstructed images from Figs. 2(a) and 2(b). These images were acquired using a similar optical configuration as the edge scans except that the sample was positioned 0.4 mm downstream from the focus where the beam is 1 μm wide [107 μm × 250 μm ( $H \times V$ ) aperture defining slits].

To take into account partial coherence effects, we reconstructed the ptychographic data set using a decomposition of the probe in orthogonal modes [28,29]. Further details are provided in Supplement 1. The magnitudes of the retrieved beam modes are shown in Figs. 2(c)–2(e). The power distribution of the modes indicated on the images shows that the dominant mode comprises 87% of the power. Figures 2(f)–2(h) show the respective Fourier transforms of the modes in Figs. 2(c)–2(e) and help to understand the contribution of the different modes. The Fourier transform of the dominant mode [Fig. 2(f)], which represents an image of the pupil opening, is consistent with a uniform intensity distribution of the incoming beam on the aperture.

Such partial-coherence effects do not significantly affect our measurements of the beam shape in the focus, which can be confirmed by the similarity in intensity between the dominant mode [Fig. 2(i)] and the total sum of the modes [Fig. 2(k)]. Although the secondary modes are important to take into account the partial-coherence effects, their contribution to the total power of the beam is only about 13%. Additionally, the focal spot size obtained from the propagated wavefront using only the dominant mode is the same as the one obtained from the incoherent sum of all the mode intensities (see Supplement 1).

Finally, the Fresnel propagation of the wavefront retrieved by ptychography from the sample position to the focus position is shown in Figs. 3(a) and 3(b) for, respectively, the horizontal and vertical cross-sections along the optical axis. Dashed lines indicate the position of the focus. Figure 3(c) shows the amplitude of the wavefront in the focus position, which shows a strong 2D sinc function character, as expected from the square aperture defining slits. The inset shows a zoomed-in area of the central part. Figure 3(d) shows the intensity along the horizontal and vertical directions integrated along the orthogonal direction.

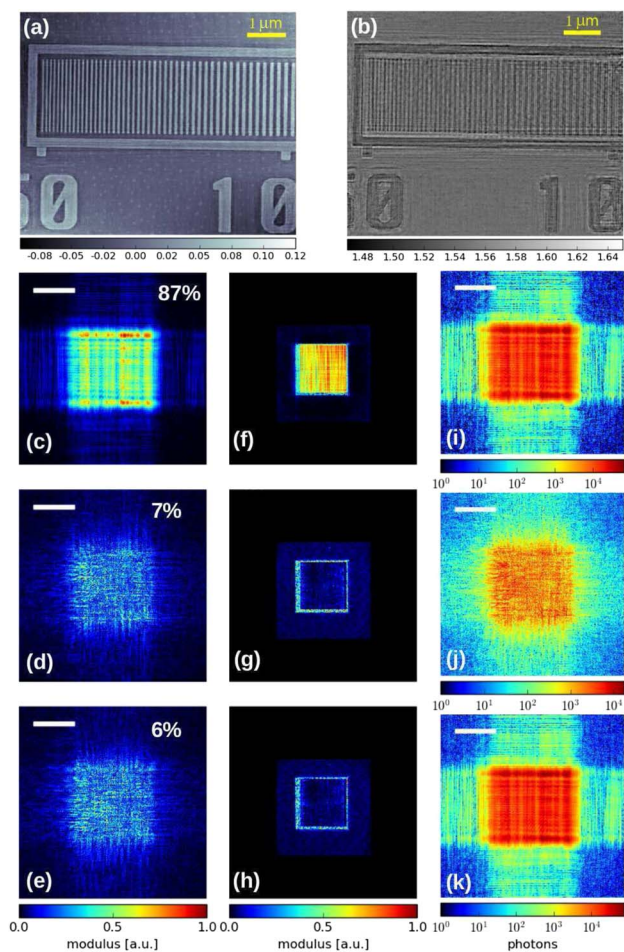


**Fig. 2.** Reconstructed object and x-ray beam at the sample position obtained from ptychographic measurements with a 200-nm-thick gold lithographic structure using high-energy x-rays (33.6 keV). (a) Phase-contrast image. (b) Amplitude image. Panels (c)–(e) show three orthogonal modes decomposed from the probe. The dominant mode is (c) with (d) and (e) in decreasing order. Panels (f)–(h) show the respective Fourier transforms of the probes in panels (c)–(e). (i) Intensity contribution of the principal mode. (j) Intensity contributions of the other modes. (k) Incoherent sum of the intensities of all modes. The white scale bars represent 500 nm.

This corresponds to the intensity distribution of the XRF edge scans in the focus position. By fitting the dominant peak using a Gaussian function [see Fig. 3(d)], we show that most of the photons are concentrated in an area of about  $12 \text{ nm} \times 13 \text{ nm}$  in FWHM. A simulated intensity profile of an ideal optical system is shown in Fig. 3(d) alongside the data, demonstrating a very good agreement. Those values are, within experimental errors, in good match with the diffraction limit calculated for aperture defining slits of  $107 \mu\text{m} \times 250 \mu\text{m}$  ( $H \times V$ ), which is  $13 \text{ nm} \times 13 \text{ nm}$  ( $H \times V$ ). Although there are some side lobes in the obtained beam at the focus, the main peak carries most of the total intensity and can, therefore, be representative of the beam size. Such additional side lobes, in addition to the imperfection of the sharp-edge test object, may explain the previous higher values obtained by edge scans.

In order to verify that the beam shape retrieved by ptychography followed by Fresnel propagation corresponds to the real shape of the beam at the focus position, we performed an

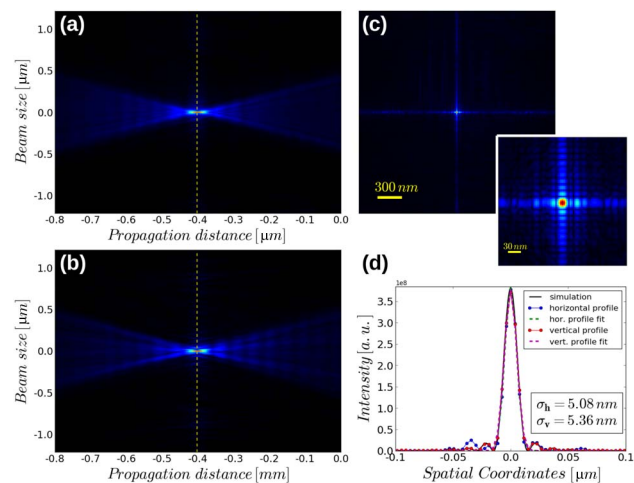


**Fig. 3.** X-ray wavefront characterization and focus size. (a) Vertical cross-section of the propagation of the wavefront. (b) Horizontal cross-section of the propagation of the wavefront. In (a) and (b), the sample is at position 0 and the focus is indicated by the dashed yellow line. (c) Beam at the focus position. The inset displays a zoomed-in view of the central part. (d) Horizontal and vertical profiles of the intensity of the beam at the focus position plotted together with a simulated profile of an ideal optical system. The FWHM values calculated by  $2\sqrt{2} \log(2)\sigma$  were 12.0 nm for the horizontal focus and 12.6 nm for the vertical focus.

XRF experiment in the focus position on the same gold structure from Fig. 2. We measured a flux of  $6 \times 10^9$  photons per second. The beam shape dominates the point-spread function in the XRF imaging. Therefore, by performing the deconvolution of the image using the experimentally obtained beam shape in focus, we could demonstrate a substantial improvement of the sharpness of the XRF image shown in Fig. 4. Figure 4(a) shows the results of the XRF experiment and Fig. 4(b) shows the result after the deconvolution. This clearly indicates that the beam shape presented in Fig. 3 corresponds to the beam in the focus during the XRF experiment. The insets in Fig. 4 highlight a region where we can better resolve the separation of the 50-nm-wide lines.

We devised a nanoprobe that confines 6 billion high-energy x-ray photons per second in an area of  $12 \text{ nm} \times 13 \text{ nm}$ . This focal spot size is diffraction-limited and breaks a barrier of focal spot size and brightness at energies above 20 keV. Such a nanoprobe enables better resolved imaging where the use of high-energy x-rays is necessary. It is routinely available for XRF and phase-contrast nanoscience-related studies at the ID16A nanoimaging beamline of the ESRF. The high flux is essential to be able to

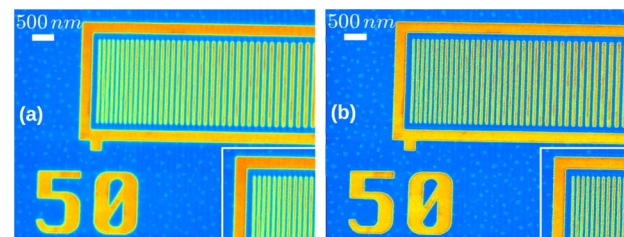


**Fig. 4.** Deconvolution of an XRF image of the L-line fluorescence of a 200-nm-thick gold lithographic structure using high-energy x-rays (33.6 keV). (a) Original image. (b) Deconvolved image. The insets to the bottom right highlight a region for comparison.

probe very small, localized areas of the specimen with enough sensitivity in fluorescence and diffraction experiments or weak variations of electron density in phase-contrast x-ray imaging. This is the case for XRF excitation of elements with high binding energies such as iodine in biomedical applications. Also, the new nanoprobe will allow imaging highly absorbing thick samples, commonly found in energy-related materials or packaged semiconductor devices.

The advanced KB mirror system proved its capability of efficiently focusing a high-energy beam to a very small spot. We showed that x-ray ptychography can yield the wavefront in a more reliable way than fluorescence scans across a sharp edge. The deconvolution of an XRF image indicates the accuracy of the retrieved beam. The achievements we made with our x-ray optics and optimized end station represent significant advances in technological capability and applicability relative to previous developments, opening new venues in many interdisciplinary fields. The resolution level reached here with hard x-rays offers the possibility of performing x-ray imaging experiments with resolution higher than super-resolution optical microscopy techniques without the need of any optical fluorescence markers. The present achievement is, therefore, not only of significant interest to the large x-ray optics and x-ray imaging community, but will also be appreciated by many research fields including the life sciences and material sciences.

**Acknowledgment.** The authors acknowledge the technical support of L. Andre, R. Baker, F. Villar, A. Vivo, C. Jarnias, and O. Hignette. The sharp-edge Nickel structure was made using electron-beam lithography by J. L. Thomassin and T. Charvolin at the PTA, Upstream Technological Platform, Minattec, CEA Grenoble.

See [Supplement 1](#) for supporting content.

## REFERENCES

1. D. A. Shapiro, Y.-S. Yu, T. Tyliczszak, J. Cabana, R. Celestre, W. Chao, K. Kaznatcheev, K. L. David, F. Maia, S. Marchesini, Y. S. Meng, T. Warwick, L. L. Yang, and H. A. Padmore, *Nat. Photonics* **8**, 765 (2014).
2. G. E. Ice, J. D. Budai, and J. W. L. Pang, *Science* **334**, 1234 (2011).
3. A. Sakdinawat and D. Attwood, *Nat. Photonics* **4**, 840 (2010).
4. J. Lawrence, G. Swerhone, J. Dynes, D. Korber, and A. Hitchcock, *J. Microsc.* **261**, 130 (2016).
5. P. Bleuet, P. Gergaud, L. Lemelle, P. Bleuet, R. Tucoulou, P. Cloetens, J. Susini, G. Delette, and A. Simionovici, *TrAC Trends Anal. Chem.* **29**, 518 (2010).
6. S. Matsuyama, M. Shimura, H. Mimura, M. Fujii, H. Yumoto, Y. Sano, M. Yabashi, Y. Nishino, K. Tamasaku, T. Ishikawa, and K. Yamauchi, *X-Ray Spectrom.* **38**, 89 (2009).
7. J. Cauzid, P. Philippot, P. Bleuet, A. Simionovici, A. Somogyi, and B. Golosio, *Spectrochim. Acta B* **62**, 799 (2007).
8. B. Golosio, A. Somogyi, A. Simionovici, P. Bleuet, J. Susini, and L. Lemelle, *Appl. Phys. Lett.* **84**, 2199 (2004).
9. I. Letard, R. Tucoulou, P. Bleuet, G. Martínez-Criado, A. Somogyi, L. Vincze, J. Morse, and J. Susini, *Rev. Sci. Instrum.* **77**, 063705 (2006).
10. P. Kirkpatrick and A. V. Baez, *J. Opt. Soc. Am.* **38**, 766 (1948).
11. A. V. Baez, *J. Opt. Soc. Am.* **51**, 405 (1961).
12. A. Snigirev, V. Kohn, I. Snigireva, and B. Lengeler, *Nature* **384**, 49 (1996).
13. H. C. Kang, H. Yan, R. P. Winarski, M. V. Holt, J. Maser, C. Liu, R. Conley, S. Vogt, A. T. Macrander, and G. B. Stephenson, *Appl. Phys. Lett.* **92**, 221114 (2008).
14. H. Yan, V. Rose, D. Shu, E. Lima, H. C. Kang, R. Conley, C. Liu, N. Jahedi, A. T. Macrander, G. B. Stephenson, M. Holt, Y. S. Chu, M. Lu, and J. Maser, *Opt. Express* **19**, 15069 (2011).
15. H. Mimura, S. Handa, T. Kimura, H. Yumoto, D. Yamakawa, H. Yokoyama, S. Matsuyama, K. Inagaki, K. Yamamura, Y. Sano, K. Tamasaku, Y. Nishino, M. Yabashi, T. Ishikawa, and K. Yamauchi, *Nat. Phys.* **6**, 122 (2010).
16. F. Seiboth, M. Kahnt, M. Scholz, M. Seyrich, F. Wittwer, J. Garrevoet, G. Falkenberg, A. Schropp, and C. G. Schroer, *Proc. SPIE* **9963**, 99630P (2016).
17. C. Morawe, R. Barrett, P. Cloetens, B. Lantelme, J.-C. Peffen, and A. Vivo, *Proc. SPIE* **9588**, 958803 (2015).
18. JTEC Corporation, <https://www.j-tec.co.jp/english/>.
19. E. McLeod and A. Ozcan, *Rep. Prog. Phys.* **79**, 076001 (2016).
20. S. W. Hell, *Science* **316**, 1153 (2007).
21. A. E. Siegman, M. W. Sasnett, and T. F. Johnston, *IEEE J. Quantum Electron.* **27**, 1098 (1991).
22. J. C. da Silva and A. Menzel, *Opt. Express* **23**, 33812 (2015).
23. C. M. Kewish, M. Guizar-Sicairos, C. Liu, J. Qian, B. Shi, C. Benson, A. M. Khounsary, J. Vila-Comamala, O. Bunk, J. R. Fienup, A. T. Macrander, and L. Assoufid, *Opt. Express* **18**, 23420 (2010).
24. P. Thibault, M. Dierolf, O. Bunk, A. Menzel, and F. Pfeiffer, *Ultramicroscopy* **109**, 338 (2009).
25. P. Thibault, M. Dierolf, A. Menzel, O. Bunk, C. David, and F. Pfeiffer, *Science* **321**, 379 (2008).
26. H. M. L. Faulkner and J. M. Rodenburg, *Phys. Rev. Lett.* **93**, 023903 (2004).
27. J. W. Goodman, *Introduction to Fourier Optics* (Roberts & Company, 2005).
28. P. Thibault and A. Menzel, *Nature* **494**, 68 (2013).
29. B. Enders, M. Dierolf, P. Cloetens, M. Stockmar, F. Pfeiffer, and P. Thibault, *Appl. Phys. Lett.* **104**, 171104 (2014).